Journal of Petroleum Science and Engineering 195 (2020) 107886

Contents lists available at ScienceDirect

Journal of Petroleum Science and Engineering

journal homepage: http://www.elsevier.com/locate/petrol

Accelerating flash calculations in unconventional reservoirs considering capillary pressure using an optimized deep learning algorithm

Tao Zhang [a], Yiteng Li [a], Shuyu Sun [a,*], Hua Bai [b]

[a] Computational Transport Phenomena Laboratory (CTPL), King Abdullah University of Science and Technology (KAUST), Thuwal, 23955-6900, Saudi Arabia
[b] Petrochina Beijing Oil and Gas Pipeline Control Center, 9 Dongzhimen North Street, Dongcheng District, Beijing, 100007, China

ARTICLE INFO

Keywords:
Phase equilibrium
NVT Flash calculation
Capillary pressure
Deep learning algorithm

ABSTRACT

An increasing focus was placed in the past few decades on accelerating flash calculations and a variety of acceleration strategies have been developed to improve its efficiency without serious compromise in accuracy and reliability. Recently, as machine learning becomes a powerful tool to handle complicated and time-consuming problems, it is increasingly appealing to replace the iterative flash algorithm, due to the strong nonlinearity of flash problem, by a neural network model. In this study, an NVT flash calculation scheme is established with a thermodynamically stable evolution algorithm to generate training and testing data for the proposed deep neural network. With a modified network structure, the deep learning algorithm is optimized by carefully tuning neural network hyperparameters. Numerical tests indicate that the trained model is capable of accurately estimating phase compositions and states for complex reservoir fluids under a wide range of environmental conditions, while the effect of capillary pressure can be captured well. Thermodynamic rules are preserved well through our algorithm, and the trained model can be used for various fluid mixtures, which significantly accelerates flash calculations in unconventional reservoirs.

1. Introduction

Due to the increasingly attractive issues associated with the modern petroleum industry, compositional multiphase fluid flow in subsurface porous media has become a hot topic in current petroleum engineering academy (Cai et al., 2018; Lian et al., 2019; Sun and Zhang, 2020). With the growing demand for energy, an increasing focus has been shifted to unconventional resources to make up the production decline of conventional oil and gas, especially in North America and China. In addition to the technology of multistage hydraulic fracturing and horizontal well, the blowout growth of shale gas/oil production is also supported by a better understanding of flow mechanisms in shale and tight rock formations (Zhang et al., 2019a). Phase behavior modeling plays an important role since the change of reservoir fluid properties could affect flow mechanisms and displacement processes. Therefore, it is important to estimate phase compositions of reservoir fluids as further analysis on physical and thermodynamic properties can only be evaluated based on a reliable and consistent description of the phase composition distributions (Wang et al., 2019a; Wang and Sheng, 2018; Zhang and Sun, 2019). Moreover, capillary effect cannot be ignored any more when modeling phase behaviors in unconventional reservoirs, since the nano-scale pores yield a large capillary pressure. Surface tension, which is the main cause of capillarity with strong wettability preference, has also been recognized as a physical property related to the phase properties and behaviors of fluid mixtures. In a word, an accurate and reliable simulation of multi-component, multi-phase fluid flow in unconventional reservoir requires flash calculation accounts for the effect of capillary pressure (Sun, 2019).

Flash calculation can be conducted at different variable specifications (Michelsen, 1999). A well-developed flash calculation technique is established at given chemical compositions (N), pressure (P) and temperature (T), which is called "NPT" flash. Numerous efforts have been made to improve the accuracy and robustness of this flash scheme, either with or without capillary pressure (Michelsen, 1982a, 1982b; Sherafati and Jessen, 2017; Sandoval et al., 2016), making it popular in research and extensively applied in engineering problems. However, when capillary effect is taken into consideration, pressure has to be specified to a certain phase, making volume-based NPT flash schemes more suitable to investigate the effect of pore size on phase behaviors in nanopores (Sandoval et al., 2019; Nichita, 2019). Moreover, in the recent years, another flash calculation scheme has been rapidly developed with fixed chemical compositions (N), volume (V) and temperature

* Corresponding author.
E-mail address: shuyu.sun@kaust.edu.sa (S. Sun).

https://doi.org/10.1016/j.petrol.2020.107886
Received 29 December 2019; Received in revised form 30 May 2020; Accepted 2 September 2020
Available online 15 September 2020

(*T*), which is known as NVT flash (Kou et al., 2018, 2020; Souza et al., 2006; Castier, 2014). It has been successfully applied to model phase behaviors of muticomponent mixtures, as well as complex reservoir fludis, in the presence of capillary pressure (Kou et al., 2018; Li et al., 2018; Zhang et al., 2019b). As an alternative of the well-developed NPT flash, Successive Substitution Iteration (SSI) method has been introduced to solve NVT flash problems, while an appropriately defined thermodynamic function was proposed similar to the fugacity defined in conventional pressure-based formulations (Mikyška and Firoozabadi, 2011). Later, such functions have been introduced in a very simple way to isolate different independent variables in the stationary condition for volume-based NPT and NVT flash calculations (Nichita, 2017, 2018a, 2018b). In addition, Newton's method has also been extensively employed in NVT flash schemes combining with a modified Cholesky factorization of the Hessian matrix to solve the Helmholtz free energy minimization problems (Jindrová and Mikyška, 2013). Recently, a Newton method and several formal links between various methods for the NVT flash has been discussed in detail (Nichita, 2018c). It is shown that the SSI method, introduced as a fixed point method in (Mikyška and Firoozabadi, 2011), corresponds to a modified gradient step in an unconstrained minimization of the Helmholtz free energy with respect to mole numbers. Except for these extensions from conventional NPT flash algorithms, a dynamic model was proposed based on diffuse interface (DI) theory to describe phase behaviors under the NVT flash framework (Kou et al., 2018; Li et al., 2018). As a pore scale algorithm, this dynamic NVT flash calculation technique can capture the diffusive interface behaviors if desired, and save a lot of CPU time compared with molecular simulation with a similar level of reliability.

However, the current petroleum industry is requiring an accurate description of phase behaviors of complex reservoir fluids, which also makes the high-resolution compositional reservoir simulation that involves millions of grid blocks a dramatically challenging job, since a large amount of CPU time of compositional simulation has been reported to be spent on flash calculations. Therefore, it is imperative to speed up flash calculation without too much compromise in accuracy and reliability. In the last three decades, a large number of studies devoted to apply and improve reduction methods in which the to-be-solved equations and variables are less than the original flash problems so as to improve computational efficiency (Michelsen, 1986; Jensen and Fredenslund, 1987; Hoteit and Firoozabadi, 2006; Li and Johns, 2006; Nichita and Graciaa, 2011; Nichita and Petitfrere, 2013; Nichita and Minescu, 2004; Petitfrere and Nichita, 2015a, 2015b). Numerous efforts have been made to investigate and evaluate the performance of various reduction methods, but their applicability and efficiency are still questioned (Haugen and Beckner, 2011; Michelsen et al., 2013). A comparative study of the reduced-variables-based flash and conventional flash was presented in (Michelsen et al., 2013), concluding that the reduction methods exhibit a better computational efficiency than the conventional method only if the number of components is large enough. In addition to the reduced models, the non-iterative method is another option to accelerate flash calculations (Wang and Stenby, 1994), and many other approches, like shadow region method (Rasmussen et al., 2003), compositional space method (Yan et al., 2017) and sparse grid method (Wu and Chen, 2018), have been developed by reducing the cost of either stability test or phase split calculation. Recently, with the worldwide popularity on artifical intelligence, artificial neural network (ANN) has also been increasingly applied to accelerate flash calculations. Gaganis and Varotsis developed regression models using ANN to predict equilibrium coefficients in both conventional and reduced approach (Gaganis and Varotsis, 2012, 2014). Later, they presented a new classification technique using two simplified discriminating functions to achieve rapid stability determination (Gaganis, 2018). In (Wang et al., 2019b), machine learning models are trained using ANNs for both stability test and phase split calculation, in which the ANN model for stability testing predicts the saturation pressure and the other ANN model provides initial mole fractions and equilibrium coefficients for phase split calculations.

In this study, a dynamic NVT flash scheme is established based on the diffuse interface theory with a thermodynamically-stable algorithm constructed by convex splitting of Helmholtz free energy and positive definite Onsager coefficient matrix. With the proposed dynamic model, reliable flash data can be obtained and used as the training input for the deep neural network. In comparison to our previous work (Li et al., 2019a), a modification is made to improve the training efficiency and reliability for the proposed deep learning model. Techniques including dropout and batch normalization are used to reduce the over-fitting issue and speed up the data training. To achieve a better prediction accuracy, network hyperparameters are optimized and then the optimal network is applied to accelerate flash calculations considering capillary pressure. With the well trained model, the effect of capillary pressure on phase equilibrium compositions and states can be captured well, which benefits the application in unconventional reservoirs. The remainder of this paper is organized as follows. In Section 2, a thermodynamically stable dynamic model is established under NVT flash framework to generate training and testing data. Deep learning algorithms are investigated in Section 3 with hyperparameter tuning and the performance of the optimized network structure on cases with capillary pressure is discussed. At the end, we make some conclusions on acceleration of flash calculation using fully connected deep neural network.

2. Thermodynamic consistent flash calculation scheme considering capillary pressure

The research on the effect of capillary pressure on phase behavior has been conducted more than twenty years and numerous efforts have been made to improve phase behavior modeling in nanopores (Brusilovsky, 1992; Sandoval et al., 2016; Nojabaei et al., 2013). As the pore size decreases, the capillary effect becomes increasingly significant, and moreover the interactions between fluid molecules and pore walls start to impact physical properties of reservoir fluids so that these interactions are nonnegligible. It was pointed out that the neglected molecule-pore wall interactions may result in a failure to accurately estimate phase behavior and fluid properties at smaller pore sizes (Teklu et al., 2014; Jin et al., 2013). However, same as the most studies, we are more interested in the effect of capillary pressure on phase behavior modeling. Thus, in this section, a dynamic flash calculation scheme is established to consider the capillary effect and preserve the consistency with thermodynamic laws.

2.1. Mole and volume evolution equations

Diffuse interface modeling is a well-developed technique for multicomponent multi-phase flow simulation with advantage of the accurate description of phase behaviors especially on the diffusive interfaces (Zhu et al., 2019). To design a dynamic flash model, here the diffuse interface model is simplified by assuming a curved interface with zero thickness. In order to describe bulk phase equilibrium under the NVT flash framework, Helmholtz free energy is minimized instead of the Gibbs free energy in NPT flash schemes. Let's consider a fluid mixture of *M* components occupies volume *V* at temperature *T*. We denote by $f(\boldsymbol{n})$ the Helmholtz free energy density which has the following form

$$f(\mathbf{n}) = RT\sum_{i=1}^{M} n_i(\ln n_i - 1) - nRT\ln(1-bn) + \frac{a(T)n}{2\sqrt{2}b}\ln\left(\frac{1+\left(1-\sqrt{2}\right)bn}{1+\left(1+\sqrt{2}\right)bn}\right), \tag{1}$$

where $n = \sum_i n_i$ is the overall molar density. For a vapor-liquid two-phase system, the Helmholtz free energy $F(\boldsymbol{n})$ can be formulated as

$$F = f(\boldsymbol{n}_G)V_G + f(\boldsymbol{n}_L)V_L \tag{2}$$

where $\boldsymbol{n}_\alpha = \boldsymbol{N}_\alpha/V_\alpha$, $\alpha = G,\ L$. In the above formulations, $\boldsymbol{n}_\alpha =$

$[n_{1,\alpha}, \ldots, n_{M,\alpha}]^T$ denotes the vector fo molar density, $N_\alpha = [N_{1,\alpha}, \ldots, N_{M,\alpha}]^T$ denotes the vector of mole number and V_α denotes the volume of phase α respectively. In addition, there remains two constraints on mole numbers and volume as $N_{i,G} + N_{i,L} = N_i$ and $V_G + V_L = V$.

It can be stated from the first law of thermodynamics that

$$\frac{d(U+E)}{dt} = \frac{dW}{dt} + \frac{dQ}{dt}, \tag{3}$$

where U is the internal energy, E is the kinetic energy, Q is the heat transfer into the system and W is the work done by the force. Note that the total entropy S can be split into two parts, one is the entropy of the system, S_{sys} and the other one is the entropy of the surroundings, S_{surr}. The relation between S_{surr} and Q can be represented by

$$dS_{\text{surr}} = -\frac{dQ}{T}. \tag{4}$$

Using the relation of $U = F + TS_{\text{sys}}$, an entropy production equation can be formulated as below

$$\overset{\frac{dS}{dt} = \frac{dS_{\text{sys}}}{dt} + \frac{dS_{\text{surr}}}{dt} = \frac{dS_{\text{sys}}}{dt} - \frac{1}{T}\frac{dQ}{dt}}{= \frac{dS_{\text{sys}}}{dt} - \frac{1}{T}\left(\frac{d(U+E)}{dt} - \frac{dW}{dt}\right) = -\frac{1}{T}\frac{d(F+E)}{dt} + \frac{1}{T}\frac{dW}{dt}}. \tag{5}$$

In order to take into account the capillary effect in Eq. (5), it is important to define the work done by capillary pressure. If we assume capillary pressure is constant along the curved interface, the work done by capillary pressure is given by

$$\frac{\mathrm{d}W}{\mathrm{d}t} = -p_G\frac{\mathrm{d}V_G}{\mathrm{d}t} - p_L\frac{\mathrm{d}V_L}{\mathrm{d}t} = -p_G\frac{\mathrm{d}V_G}{\mathrm{d}t} + p_L\frac{\mathrm{d}V_G}{\mathrm{d}t} = -p_c\frac{\mathrm{d}V_G}{\mathrm{d}t}\ , \tag{6}$$

where p_G and p_L represent the pressure of vapor phase and liquid phase respectively. Note that $dV_G + dV_L = 0$ since the total volume is fixed. In this study, the capillary pressure is computed by the Young-Laplace equation

$$p_c = \frac{2\sigma\cos\theta}{r}, \tag{7}$$

where the interfacial tension σ is given by the Weinaug-Katz correlation (Weinaug and Katz, 1943)

$$\sigma = \left[\sum_{i=1}^{M}[\mathbf{P}]_i\left(n_{i,L} - n_{i,G}\right)\right]^4. \tag{8}$$

For a standalone flash calculation, the kinetic energy E in Eq. (5) is assumed zero. By substituting Eq. (6) and the time derivative of Helmholtz free energy

$$\frac{\mathrm{d}F}{\mathrm{d}t} = \sum_{i=1}^{M}(\mu_i(\mathbf{n}_G) - \mu_i(\mathbf{n}_L))\frac{\partial N_{i,G}}{\partial t} + (p_L - p_G)\frac{\partial V_G}{\partial t} \tag{9}$$

into Eq. (5), there exists a symmetrical matrix $\boldsymbol{\Psi} = (\psi_{ij})_{i,j=1}^{M+1}$ that follows the Onsager's reciprocal principle, leading to the following mole and volume evolution equations

$$\frac{\partial N_{i,G}}{\partial t} = \sum_{j=1}^{M}\psi_{i,j}\left(\mu_j(\boldsymbol{n}_L) - \mu_j(\boldsymbol{n}_G)\right) + \psi_{i,M+1}(p_G - p_L - p_c), 1 \le i \le M\ , \tag{10}$$

$$\frac{\partial V_G}{\partial t} = \sum_{j=1}^{M}\psi_{M+1,j}\left(\mu_j(\boldsymbol{n}_L) - \mu_j(\boldsymbol{n}_G)\right) + \psi_{M+1,M+1}(p_G - p_L - p_c)\ . \tag{11}$$

It is noted that mole numbers and volume of the vapor phase are selected as the primary variables.

In order to keep the increase of the total entropy, which is required by the second law of thermodynamics, the Onsager coefficient matrix, $\boldsymbol{\Psi}$, has to be positive definite (Kou et al., 2018; Li et al., 2018). For this purpose, a simple approach is to construct a diagonal positive definite matrix with the diagonal elements defined as follows (Kou et al., 2018)

$$\psi_{i,i} = \frac{D_i N_i^t}{RT},\ i = 1, \ldots, M, \quad \psi_{M+1,M+1} = \frac{C_V^G C_V^L V}{C_V^L p_G + C_V^G p_L}\ , \tag{12}$$

where D_i is the diffusion coefficient of component i and C_V^G and C_V^L are the nonzero parameters. The corresponding evolutionary equations for moles and volume are simplified as

$$\frac{\partial N_{i,G}}{\partial t} = \frac{D_i N_i^t}{RT}(\mu_i(\boldsymbol{n}_L) - \mu_i(\boldsymbol{n}_G)), \quad i = 1, \ldots, M\ , \tag{13}$$

$$\frac{\partial V_G}{\partial t} = \frac{C_V^G C_V^L V}{C_V^L p_G + C_V^G p_L}(p_G - p_L - p_c)\ . \tag{14}$$

In addition to sequentially solving Eqs. (13) and (14), the original mole and volume evolution equations, Eqs. (10) and (11), can be simultaneously solved by introducing a generalized Onsager coefficient matrix of the following form

$$\boldsymbol{\Psi} = \begin{bmatrix} A & B \\ B^T & C \end{bmatrix}, \tag{15}$$

where $A = \partial(\mu_{i,L} - \mu_{i,G})/\partial N_{i,G}$, $B = \partial(\mu_{i,L} - \mu_{i,G})/\partial V_G = \partial(p_G - p_L)/\partial N_{i,G}$, and $C = \partial(p_G - p_L)/\partial V_G$ (Li et al., 2018). We note the proposed Onsager coefficient matrix is same as the Hessian matrix in (Nichita, 2018c) for minimizing the Helmholtz free energy if divided by RT.

To ensure the dynamic model holds the entropy-production property over iterations, convex splitting of Helmholtz free energy plays an important role in temporal discretization of mole and volume evolution equations. A semi-implicit time marching scheme is employed to construct a thermodynamically stable numerical algorithm. Specifically, the convex parts of chemical potential and Helmholtz free energy density are solved implicitly while the concave parts are solved explicitly. The detailed time discretization of Eqs. (10) and (11), as well as the convex-concave splitting of Helmholtz free energy density and chemical potential, can be found in (Li et al., 2018) and they are not elaborated in this work. It is worth noting a modified Cholesky factorization has to be used to preserve the positive definiteness of the Onsager coefficient matrix if the matrix itself is not sufficiently positive definite. Also, a line search scheme is used to keep the solution stay inside the physical range and meanwhile safeguard the increase of the total entropy in the system over iterations.

3. Deep learning algorithm

The basic mechanism of using a deep neural network to estimate the equilibrium composition is to represent the underlying correlations between input and output thermodynamic properties. These correlations are obtained and unearthed through a process analogous to the biological nervous system, while the capability to handle practical engineering problems are determined by the network structure and hyperparameters. A fully connected deep neural network is applied in this paper and the main network structure is the same as the one used in our previous work (Li et al., 2019a; Zhang et al., 2020). In comparison, a modification is introduced to replace half of the original output parameters by a coefficient ϕ, namely the mole fraction of vapor phase, which protects the material balance from being violated by respecting a unique phase mole fraction value. Only the mole fractions of vapor components Y_i remain and consequently the total output parameters are almost halved, which we believe can greatly improve the training efficiency especially for complex fluid mixtures with a large number of components. The input parameters remain the same as previously used in (Li et al., 2019a) since this is currently the best manner to represent the critical thermodynamic properties of various components. The new network structure is illustrated by a schematic diagram in Fig. 1. To demonstrate the performance of the proposed deep learning algorithm, two real reservoir fluids are considered, including a 5-component

Bakken oil (C_1, C_{2-4}, C_{5-7}, C_{8-9} and C_{10+}) and an 8-component Eagle-Ford oil (C_1, C_2, C_3, C_4, C_5, C_{6-7}, C_{7+} and C_{13+}). The detailed compositional parameters are included in (Li et al., 2019a). It should be pointed out that in this work totally 40401 data points are generated by NVT flash calculation, in which 90% of the data points are used for training and the remaining 10% data are used for testing.

After designing the new deep neural network structure, now we briefly describe how to train a neural network on this problem. As shown in Fig. 1, the model takes the key features as input, and the key parameters of the trained model are the weights of each layer, which directly determines the final output. Initially, random weights are placed on each node and the output values are meaningless with very large errors. Iterating the training process is then expected to optimize the model's weights by minimizing the variation between the output value and ground truth data as small as possible. Such variation is called loss and in this paper the mean squared error of the output is used as the loss function. The training process can be illustrated by the decline curve of loss function, as shown in Fig. 2.

It can be seen that the loss of the trained model decreases significantly at first, due to the randomly initialized weights, and then gradually to a small value, which means that the trained model becomes much more meaningful and useful. Fluctuations are hard to avoid so that sufficient training steps are required to ensure the accuracy. After the loss function converges, the testing dataset will be fed into the trained model to oversee its performance, e.g. the estimation error. In this paper, the mean squared absolute error and mean squared relative error are used to evaluate the trained models. The mean squared absolute error is calculated as the averaged squared variance of prediction results and ground truth data (iterative flash results). The mean squared relative error is calculated via the mean squared absolute error divided by the squared average of ground truth. Optimization on the network structure and deep learning techniques are needed to accelerate the loss convergence in order to improve the training efficiency and estimation reliability.

3.1. Network optimization

The correlations behind the thermodynamic properties are expected to be captured from the messages transferred through the activation layers and this specific hierarchical structure is capable of extracting meaningful patterns and features and learning the correlation rules underneath the enormous flash calculation data. No independent phase stability test is needed due to the strong capacity of this deep learning algorithm on performing phase splitting calculation and phase stability test together using a single neural network. Compared with the preceding works (Wang et al., 2019b; Gaganis, 2018; Gaganis and Varotsis, 2014) to accelerate flash calculation using machine learning models, our algorithm is more efficient in determining the stability of feed compositions without additional phase stability test preserved as the prevailing flash frameworks. The total number of phases at equilibrium (N) is output at the regression layer and we can determine whether the mixture is at the single-vapor state or single-liquid state by checking the value of ϕ if $N = 1$.

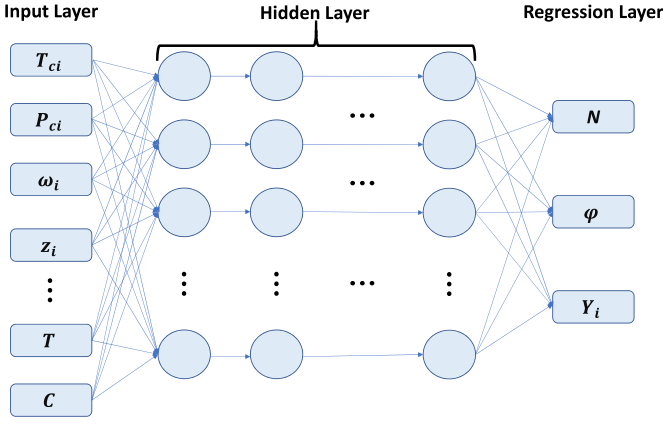

Fig. 1. Schematic diagram of the optimized fully connected deep neural network.

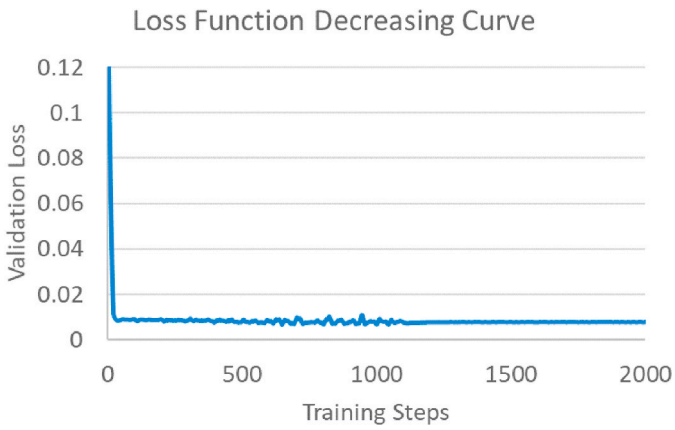

Fig. 2. The decline curve of the loss function in the training process.

As the iterative NVT flash calculation results are used as the training and testing data, the insufficient data problem of using experimental data as ground truth can be overcome and the deviations are computed by a mean squared error between flash calculation results and network predictions. Even though we can obtain as much data as needed without too much cost, overfitting is still an issue which is difficult to be fully avoided. In previous studies using experimental data as ground truth (Li et al., 2019b), the overfitting problem occurs mainly due to the insufficient data used for optimizing the numerous hyperparameters on the neural nodes. Such unsatisfactory predictions cannot be resolved easily because it is expensive to get sufficient experimental data in a uniformed format. This insufficient data problem can be overcome when flash calculation results are used as the ground truth (Li et al., 2019a), but more constraints are expected to protect the neural network performance by reducing the freedom. A delicate approach was proposed in (Li et al., 2019b), with an additional regularization term introduced to penalize the large weights if the model is overfitted. Dropout technique is a popular approach to overcome the overfitting issue in machine learning, in which certain nodes are abandoned as well as the related connections in the training process to reduce the deep neural network freedom. In particular, dropout possibilities are evaluated independently on each node and a specified possibility threshold is assigned to determine whether the nodes and layers are removed or not. The training network is reduced in this way and restored before entering the next iteration by inserting the removed nodes and layers back. Weight initialization is another important technique to accelerate the convergence rate of training and to improve the prediction accuracy of the network. The model complexity will be reduced and prediction performance may be damaged if intermediate transformations occur when the input data variance drops significantly due to underestimated initial weights, while training failure is easy to happen if the data variance increases rapidly due to overestimated initial weights. A reliable initial weight distribution is used in this paper following Gaussian distribution so that the output data variance in the same activation layer is the same as the input data variance. This is known as the Xavier initializer with the equality $n \times var(w_i) = 1$ being satisfied, where n is the number of weights and w_i is the weight on ith node.

The network performance with different configurations and data size have been investigated in (Li et al., 2019a, 2019b; Zhang et al., 2019b), and a first trial shows acceptable prediction accuracy in which the neural network is trained with 201 × 201 input data, 5 hidden layers,

100 nodes on each layer, total 4000 iterations and activation function of "ReLU". Flash calculations for bulk phase equilibria is tested first. However, in order to adjust to the possible changes caused by new output parameters, these network hyperparameters are optimized and a significant difference has been found on the number of hidden layers. As shown in Fig. 3, the network performance with 7 hidden layers is much better than with 5 hidden layers, which indicates two more activation layers are needed to accurately capture the thermodynamic correlations in this reduced network structure. Other network configurations remain unchanged and exhibit a similar performance as before, for example, the estimation error of deep neural networks with different activation functions is illustrated in Fig. 4 and it can be seen "ReLU" is still the best in the aspect of relative errors. It is interesting to see that the absolute estimation error of the network using "ReLU" is a little larger than that using "softplus". A possible explanation on this phenomenon can be attributed to the random selections of the training and testing samples from the total input data in these two cases.

3.2. Phase behavior prediction under capillary effect

The capillary effect, which is often ignored in conventional flash problems, becomes more pronounced in unconventional reservoirs, due to the nanopores in tight and shale rock formations. As a result, fluid properties are expected to deviate from their bulk properties when capillary pressure, as well as molecules-pore wall interactions, takes effect. In this subsection, NVT flash calculations considering the effect of capillary pressure are conducted and the network hyperparameters are tuned to optimize the performance. To show the wide applicability of the optimized network configurations obtained in Section 3.1, the network performance of different number of activation layers is compared in Fig. 5. It is observed that the introduction of capillary effect has slight impact on the performance of deep neural networks with various features, but the best selection still remains the same.

A significant highlight of our deep learning algorithm stands on training the neural network to automatically determine the total phase numbers of the investigated fluid mixture at equilibrium under various environmental conditions so as to avoid additional stability test. With a single neural network structure to complete both stability test and phase split calculation, the prediction accuracy and reliability of the proposed model are validated by comparing with flash calculation results. As shown in Fig. 6, for the 5-component Bakken oil mixture, the total phase numbers predicted by the deep learning algorithm at the overall concentration of 10 mol/m^3 agree with the flash calculation results very well. At small overall concentration, with temperature increasing, the two phase mixture will transform to single vapor phase, and this reasonable phase transition is successfully captured by the deep learning algorithm.

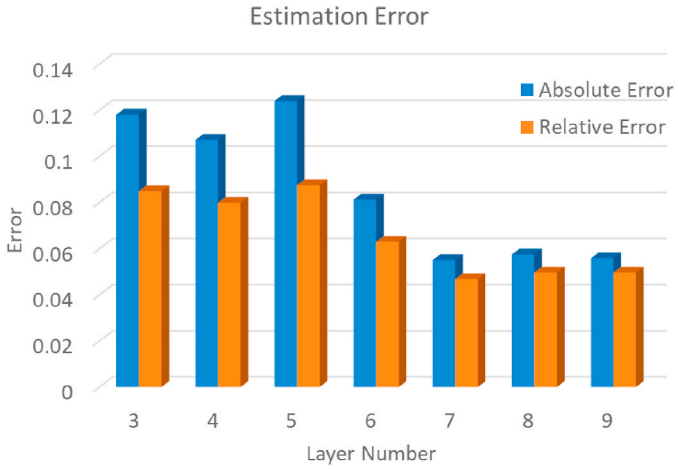

Fig. 3. Estimation error of deep neural networks with different hidden layers.

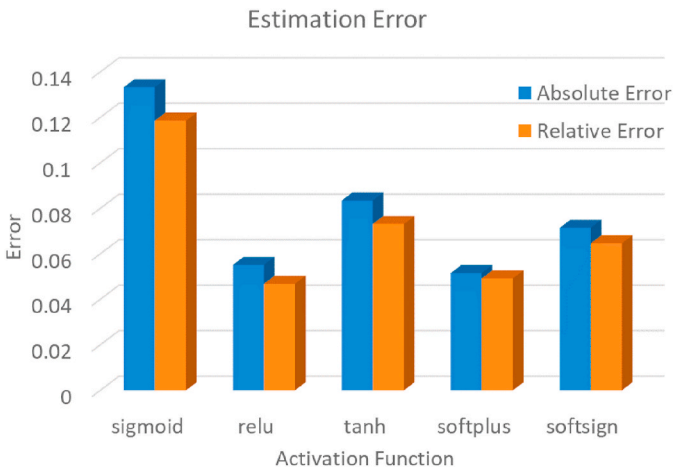

Fig. 4. Estimation error of deep neural networks with different activation functions.

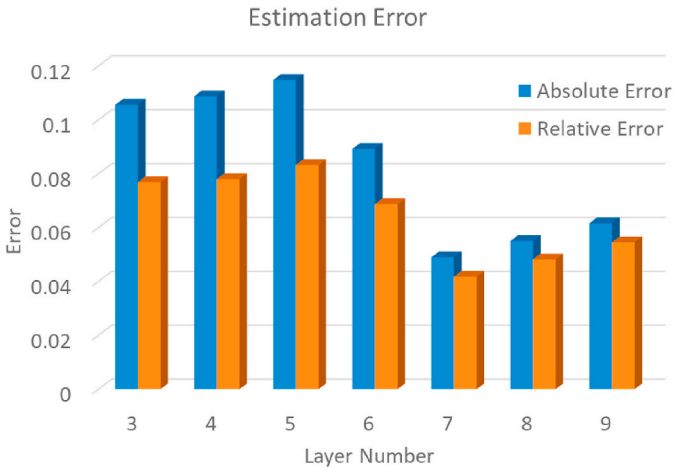

Fig. 5. Estimation error of deep neural networks with different hidden layers considering the effect of capillary pressure.

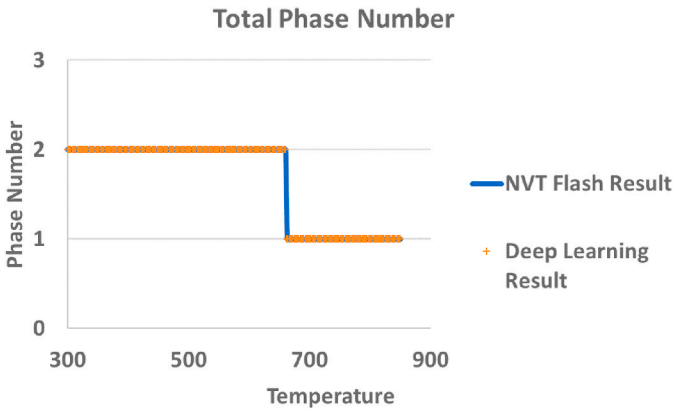

Fig. 6. Total phase numbers of the Bakken oil mixture at the overall concentration of 10.mol/m^3

The supercritical state is mainly used to indicate a region (above the critical pressure and temperature) of a pure substance where distinct liquid and gas phases do not exist. Even though it is not rigorous to define a supercritical state for multicomponent mixtures, here we

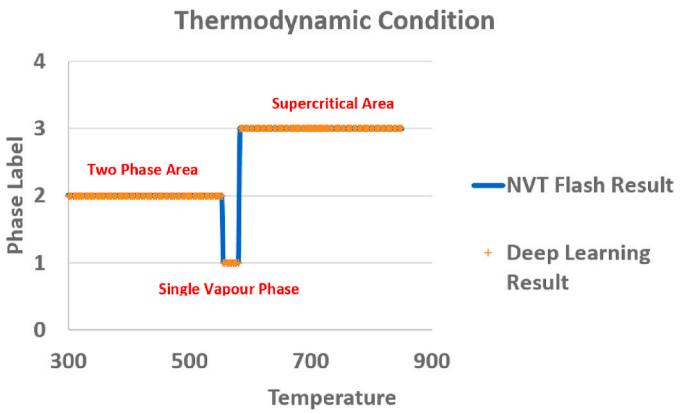

Fig. 7. Phase state of the Bakken oil mixture at the overall concentration of 5854.15 mol/m^3.

borrow this concept and consider the corresponding states lying above the critical pressure and temperature of the investigated mixture as the "supercritical" states. By checking the value of N and ϕ, we can accurately determine the phase state within the given conditions. As shown in Fig. 7, for the 5-component Bakken oil mixture, at the specified overall concentration of 5854.15 mol/m^3, the "supercritical" fluid mixture is detected by a special label of $N = 3$, and the perfect match between NVT flash results and deep learning predictions demonstrate the capability of the proposed deep neural network to correctly identify different phase states.

The effect of capillary pressure on phase behaviors are shown in Fig. 8. To construct a phase envelope under NVT flash framework, the phase boundary between single-phase and two-phase region is determined first. Then we estimate pressures along the boundary curve and draw the phase envelope. It can be seen that the bulk phase envelope is reshaped when capillary effect becomes nonnegligible. As the literature suggested, the bubble point curve is suppressed while the dew point curve is expanded outward with dew point pressure decreasing (and increasing) in the lower (and upper) branch of the dew point curve. The black point in Fig. 8 corresponds to the critical point approximately. Starting from this point, bubble point suppression is becoming more significant along the curve to lower temperature, while the dew point expansion is becoming more significant along the curve to higher temperature.

Molar compositions of each phase at equilibrium is the critical information required by multicomponent multiphase flow simulations. A comparison of molar compositions computed by NVT flash calculations and the deep learning algorithm is illustrated in Fig. 9 and Fig. 10 for the liquid phase of the 8-component Eagle Ford production at overall concentrations of 10 mol/m^3 and 2757.25 mol/m^3, respectively. The mole fractions of C_1, C_2, C_3 and nC_4 are presented in Fig. 9 and mole fractions of nC_4, C_5, C_{6-7} and C_{7+} are presented in Fig. 10, while the solid symbols represent NVT flash calculation results and the lines in the same color represent the deep learning predictions. Generally, the trained model can reproduce the flash calculation results well with acceptable errors for various fluid mixtures, indicating a good robustness and reliability of our trained model. As shown in Table 1, the mean squared absolute error (denoted by ε_a) and mean squared relative error (denoted by ε_r) for the EagleFord oil sample are both small enough to be accepted. It can be easily referred that the CPU time used for testing data batches is much smaller compared with iterative flash calculations for the same size of data. It should be pointed out that the trained model can be used to accelerate flash calculations for various fluid mixtures, so the acceleration can be validated by comparison of CPU time used in iterative flash calculation and testing using our trained model.

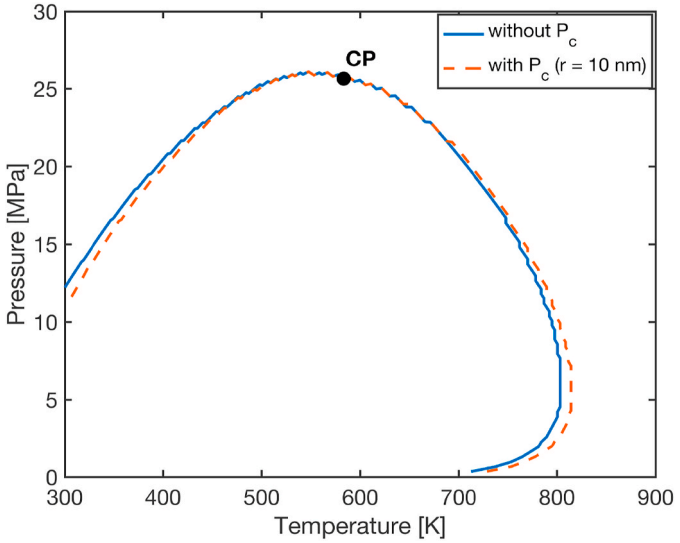

Fig. 8. Phase envelopes of the Bakken oil with and without capillary pressure.

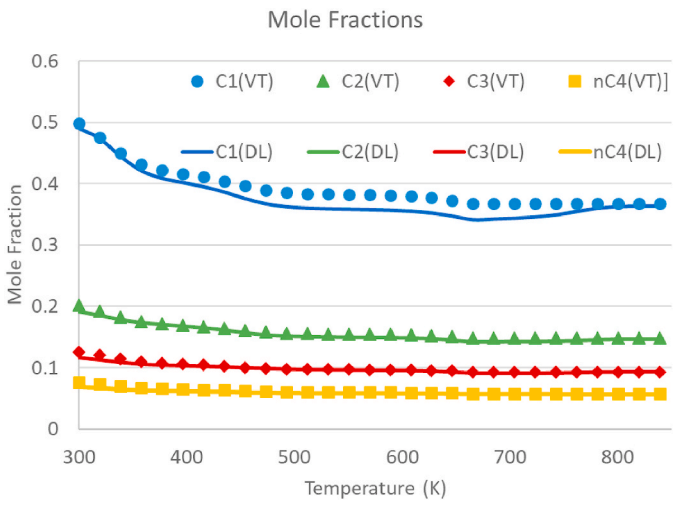

Fig. 9. Mole fractions of C_1, C_2, C_3 and nC_4 in the liquid phase of the 8-component EagleFord oil as a function of temperature at the overall concentration of 10 mol/m^3. The solid symbols and lines represent the NVT flash results and deep learning predictions, respectively.

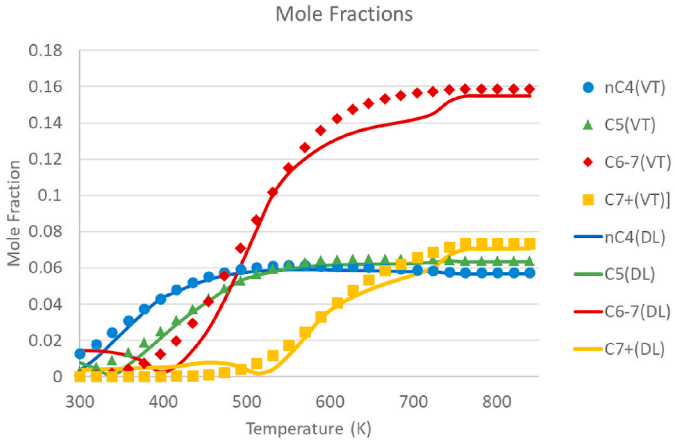

Fig. 10. Mole fractions of nC_4, C_5, C_{6-7} and C_{7+} in the liquid phase of the 8-component EagleFord oil as a function of temperature at the overall concentration of 2757.25 mol/m^3. The solid symbols and lines represent the NVT flash results and deep learning predictions, respectively.

Table 1
Performance of the deep learning algorithm.

Mixture	N_{train}	N_{test}	t_{flash} (s)	t_{train} (s)	t_{test} (s)	ε_a	ε_r
EagleFord	36361	4040	1232	1493	7.8	0.00892	0.021325

4. Conclusion and remarks

In this study, a deep learning algorithm is proposed to accelerate NVT flash calculations with capillary pressure for phase behavior modeling in nanopores. To generate training and testing data for the proposed neural network model, thermodynamically-stable mole and volume evolution equations are established to calculate equilibrium phase compositions. By halving the output parameters of our previous neural network and replacing them by a phase mole fraction value, the network structure is optimized in order to achieve the best performance. Optimal network hyperparameters are tuned as a continuous work of (Li et al., 2019a, 2019b). It is indicated that this set of fully connected neural network features can fit the purpose of accelerating flash calculations well, either with or without capillary pressure. There is a slight difference in the performance of using different numbers of hidden layers if capillary effect is considered, but a structure with seven activation layers is still the best selection. The optimized deep neural network is then tested by two reservoir fluid examples, a 5-component Bakken oil and an 8-component EagleFord oil, and exhibits good prediction accuracy for phase compositions and states. In addition, this structure also shows good efficiency and reliability for muticomponent fluid mixtures in a wide range of temperature and concentration. It is believed that this network structure is a good starting for future studies using fully connected deep neural networks to accelerate flash calculations, and the application of such network designing and training is expected in other advanced multi-phase flow simulation approaches (Sun et al., 2017; Chen et al., 2019).

CRediT authorship contribution statement

Tao Zhang: Conceptualization, Methodology, Software. **Yiteng Li:** Methodology, Software. **Shuyu Sun:** Supervision, Writing - review & editing. **Hua Bai:** Methodology, Validation.

Declaration of competing interest

The authors declare that they have no known competing financial interests or personal relationships that could have appeared to influence the work reported in this paper.

Acknowledgements

The authors thank for the support from the National Natural Science Foundation of China (No. 51874262,51936001) and the Research Funding from King Abdullah University of Science and Technology (KAUST) through the grants BAS/1/1351-01-01.

References

Brusilovsky, A.I., 1992. Mathematical simulation of phase behavior of natural multicomponent systems at high pressures with an equation of state. SPE Reservoir Eng. 7, 117–122.
Cai, J., Lin, D., Singh, H., Wei, W., Zhou, S., 2018. Shale gas transport model in 3D fractal porous media with variable pore sizes. Mar. Petrol. Geol. 98, 437–447.
Castier, M., 2014. Helmholtz function-based global phase stability test and its link to the isothermal-isochoric flash problem. Fluid Phase Equil. 379, 104–111.
Chen, H., Kou, J., Sun, S., Zhang, T., 2019. Fully mass-conservative IMPES schemes for incompressible two-phase flow in porous media. Comput. Methods Appl. Mech. Eng. 350, 641–663.
Gaganis, V., 2018. Rapid phase stability calculations in fluid flow simulation using simple discriminating functions. Comput. Chem. Eng. 108, 112–127.
Gaganis, V., Varotsis, N., 2012. Machine learning methods to speed up compositional reservoir simulation. SPE Europec/EAGE Annual Conference. Society of Petroleum Engineers.
Gaganis, V., Varotsis, N., 2014. An integrated approach for rapid phase behavior calculations in compositional modeling. J. Petrol. Sci. Eng. 118, 74–87.
Haugen, K.B., Beckner, B.L., 2011. Are reduced methods for EOS calculations worth the effort? SPE Reservoir Simulation Symposium. Society of Petroleum Engineers.
Hoteit, H., Firoozabadi, A., 2006. Simple phase stability-testing algorithm in the reduction method. AIChE J. 52, 2909–2920.
Jensen, B.H., Fredenslund, A., 1987. A simplified flash procedure for multicomponent mixtures containing hydrocarbons and one non-hydrocarbon using two-parameter cubic equations of state. Ind. Eng. Chem. Res. 26, 2129–2134.
Jin, L., Ma, Y., Jamili, A., 2013. Investigating the effect of pore proximity on phase behavior and fluid properties in shale formations. SPE Annual Technical Conference and Exhibition. Society of Petroleum Engineers.
Jindrová, T., Mikyška, J., 2013. Fast and robust algorithm for calculation of two-phase equilibria at given volume, temperature, and moles. Fluid Phase Equil. 353, 101–114.
Kou, J., Sun, S., Wang, X., 2018. Linearly decoupled energy-stable numerical methods for multicomponent two-phase compressible flow. SIAM J. Numer. Anal. 56 (6), 3219–3248.
Kou, J., Sun, S., Wang, X., 2020. A novel energy factorization approach for the diffuse-interface model with peng–robinson equation of state. SIAM J. Sci. Comput. 42 (1), B30–B56.
Li, Y., Johns, R.T., 2006. Rapid flash calculations for compositional simulation. SPE Reservoir Eval. Eng. 9, 521–529.
Li, Y., Kou, J., Sun, S., 2018. Thermodynamically stable two-phase equilibrium calculation of hydrocarbon mixtures with capillary pressure. Ind. Eng. Chem. Res. 57, 17276–17288.
Li, Y., Zhang, T., Sun, S., 2019a. Acceleration of the NVT flash calculation for multicomponent mixtures using deep neural network models. Ind. Eng. Chem. Res. 58, 12312–12322.
Li, Y., Zhang, T., Sun, S., Gao, X., 2019b. Accelerating flash calculation through deep learning methods. J. Comput. Phys. 394, 153–165.
Lian, P., Ji, B., Duan, T., Zhao, H., Shang, X., 2019. Parallel numerical simulation for a super large-scale compositional reservoir. Adv. Geo-Energy Res. 3, 381–386.
Michelsen, M.L., 1982a. The isothermal flash problem. Part I. Stability. Fluid Phase Equil. 9, 1–19.
Michelsen, M.L., 1982b. The isothermal flash problem. Part II. Phase-split calculation. Fluid Phase Equil. 9, 21–40.
Michelsen, M.L., 1986. Simplified flash calculations for cubic equations of state. Ind. Eng. Chem. Process Des. Dev. 25, 184–188.
Michelsen, M.L., 1999. State function based flash specifications. Fluid Phase Equil. 158, 61–626.
Michelsen, M., Yan, W., Stenby, E.H., 2013. A comparative study of reduced-variables-based flash and conventional flash. SPE J. 18, 952–959.
Mikyška, J., Firoozabadi, A., 2011. A new thermodynamic function for phase-splitting at constant temperature, moles, and volume. AIChE J. 57, 1897–1904.
Nichita, D.V., 2017. Fast and robust phase stability testing at isothermal-isochoric conditions. Fluid Phase Equil. 447, 107–124.
Nichita, D.V., 2018a. Volume-based phase stability testing at pressure and temperature specifications. Fluid Phase Equil. 458, 123–141.
Nichita, D.V., 2018b. A volume-based approach to phase equilibrium calculations at pressure and temperature specifications. Fluid Phase Equil. 461, 70–83.
Nichita, D.V., 2018c. New unconstrained minimization methods for robust flash calculations at temperature, volume and moles specifications. Fluid Phase Equil. 466, 31–47.
Nichita, D.V., 2019. Volume-based phase stability analysis including capillary pressure. Fluid Phase Equil. 492, 145–160.
Nichita, D.V., Graciaa, A., 2011. A new reduction method for phase equilibrium calculations. Fluid Phase Equil. 302, 226–233.
Nichita, D.V., Minescu, F., 2004. Efficient phase equilibrium calculation in a reduced flash context. Can. J. Chem. Eng. 82, 1225–1238.
Nichita, D.V., Petitfrere, M., 2013. Phase stability analysis using a reduction method. Fluid Phase Equil. 358, 27–39.
Nojabaei, B., Johns, R.T., Chu, L., 2013. Effect of capillary pressure on phase behavior in tight rocks and shales. SPE Reservoir Eval. Eng. 16, 281–289, 03.
Petitfrere, M., Nichita, D.V., 2015a. A comparison of conventional and reduction approaches for phase equilibrium calculations. Fluid Phase Equil. 386, 30–46.
Petitfrere, M., Nichita, D.V., 2015b. Multiphase equilibrium calculations using a reduction method. Fluid Phase Equil. 401, 110–126.
Rasmussen, C.P., Krejbjerg, K., Michelsen, M.L., Bjurstrøm, K.E., 2003. Increasing computational speed of flash calculations with applications for compositional, transient simulations. SPE Annual Technical Conference and Exhibition. Society of Petroleum Engineers.
Sandoval, D.R., Yan, W., Michelsen, M.L., Stenby, E.H., 2016. The phase envelope of multicomponent mixtures in the presence of a capillary pressure difference. Ind. Eng. Chem. Res. 55, 6530–6538.

Sandoval, D.R., Michelsen, M.L., Yan, W., Stenby, E.H., 2019. VT-based phase envelope and flash calculations in the presence of capillary pressure. Ind. Eng. Chem. Res. 58, 5291–5300.
Sherafati, M., Jessen, K., 2017. Stability analysis for multicomponent mixtures including capillary pressure. Fluid Phase Equil. 433, 56–66.
Souza, A.T., Cardozo-Filho, L., Wolff, F., Guirardello, R., 2006. Application of interval analysis for Gibbs and Helmholtz free energy global minimization in phase stability analysis. Braz. J. Chem. Eng. 23, 117–124.
Sun, S., 2019. Darcy-scale phase equilibrium modeling with gravity and capillarity. J. Comput. Phys. 399, 108908.
Sun, S., Zhang, T., 2020. A 6M digital twin for modeling and simulation in subsurface reservoirs. Adv. Geo-Energy Res. 4, 349–351.
Sun, D.L., Yu, S., Yu, B., Wang, P., Liu, W.J., 2017. A VOSET method combined with IDEAL algorithm for 3D two-phase flows with large density and viscosity ratio. Int. J. Heat Mass Tran. 144, 155–168.
Teklu, T.W., Alharthy, N., Kazemi, H., Yin, X., Graves, R.M., AlSumaiti, A.M., 2014. Phase behavior and minimum miscibility pressure in nanopores. SPE Reservoir Eval. Eng. 17, 396–403, 03.
Wang, X., Sheng, J.J., 2018. A self-similar analytical solution of spontaneous and forced imbibition in porous media. Adv. Geo-Energy Res. 2, 260–268.
Wang, P., Stenby, E.H., 1994. Non-iterative flash calculation algorithm in compositional reservoir simulation. Fluid Phase Equil. 95, 93–108.
Wang, H., Yuan, X., Liang, H., Chai, Z., Shi, B., 2019a. A brief review of the phase-field-based lattice Boltzmann method for multiphase flows. Capillarity 2, 33–52.
Wang, K., Luo, J., Wei, Y., Wu, K., Li, J., Chen, Z., 2019b. Artificial neural network assisted two-phase flash calculations in isothermal and thermal compositional simulations. Fluid Phase Equil. 486, 59–79.
Weinaug, C.F., Katz, D.L., 1943. Surface tensions of methane-propane mixtures. Ind. Eng. Chem. 35, 239–246.
Wu, Y., Chen, Z., 2018. The application of high-dimensional sparse grids in flash calculations: from theory to realisation. Fluid Phase Equil. 464, 22–31.
Yan, B., Wang, Y., Nasrabadi, H., Killough, J.E., Wu, K., 2017. Accelerating flash calculation using compositional space for compositional simulation. J. Petrol. Sci. Eng. 159, 1000–1008.
Zhang, T., Sun, S., 2019. A coupled Lattice Boltzmann approach to simulate gas flow and transport in shale reservoirs with dynamic sorption. Fuel 246, 196–203.
Zhang, T., Sun, S., Song, H., 2019a. Flow mechanism and simulation approaches for shale gas reservoirs: a review, 126. Transp. Porous Media, pp. 655–681.
Zhang, T., Li, Y., Sun, S., 2019b. Phase equilibrium calculations in shale gas reservoirs. Capillarity 2, 8–16.
Zhang, T., Li, Y., Li, Y., Sun, S., Gao, X., 2020. A self-adaptive deep learning algorithm for accelerating multi-component flash calculation. Comput. Methods Appl. Mech. Eng. 369, 113207.
Zhu, G., Kou, J., Yao, B., Wu, Y.S., Yao, J., Sun, S., 2019. Thermodynamically consistent modelling of two-phase flows with moving contact line and soluble surfactants. J. Fluid Mech. 879, 327–359.